Acta Crystallographica Section D
Biological Crystallography
ISSN 0907-4449

Morphology and the strength of intermolecular contacts in protein crystals

Yoshiki Matsuura[a]* and Alexander A. Chernov[b]

[a]Institute for Protein Research, Osaka University, Suita, Osaka 565-0871, Japan, and [b]Marshall Space Flight Center, NASA, Huntsville, AL 35812, USA

Correspondence e-mail: matsuura@protein.osaka-u.ac.jp

Received 12 December 2002
Accepted 19 May 2003

The strengths of intermolecular contacts (macrobonds) and the areas occupied by each contact on the molecular surface were estimated in four polymorphic modifications of lysozyme crystals based on the bond strengths between individual atomic pairs belonging to the molecules in contact. It has been shown that the periodic bond chains of these macrobonds account for the morphology of protein crystals. The Coulombic contribution to the macrobond strength has also been estimated. Making use of the contact strengths and taking into account bond hydration, crystal–water interfacial energies were also estimated for different crystal faces. The areas of all contacts are mapped on the molecular surface, making use of a polar-coordinate representation of the contact. Comparing the locations of the intermolecular contacts in the different polymorphic crystal modifications, it is shown that these contacts can form a wide variety of patches on the molecular surface. The patches are located practically everywhere on the surface except for the inside of a concave active site. It is also shown that the contacts, which frequently involve water molecules, are formed by specific intermolecular hydrogen bonds on a background of non-specific attractive electrostatic interactions. Typical values of the macrobond strength are compared with the strength of association in other protein-complex systems.

1. Introduction

In a protein molecule, the polypeptide chain is folded into a globule, with the hydrophilic amino acids mainly on the surface and the hydrophobic ones in the core. The naturally folded conformation of a protein is formed in aqueous solution, with the surface being hydrated depending on the hydration potential (Wolfenden *et al.*, 1981), in combination with other properties of folded polypeptide amino acids (Kyte, 1995). The overall process of protein crystallization (Vekilov & Chernov, 2002) is mainly governed by the nature of the protein molecules. The intermolecular contacts in the crystal lattice include groups of surface atoms bound by various kind of intermolecular forces, such as hydrogen bonds, ionic and van der Waals interactions, which frequently involve bound water molecules on the surface of the molecules. These intermolecular contacts occupy various areas on the molecular surface and have various strengths depending on the nature of the protein molecules and the crystal form.

Hen egg-white lysozyme is the most extensively studied protein with respect to protein crystal growth. It is known to crystallize in at least four different crystal systems: tetragonal, orthorhombic, monoclinic and triclinic. Crystal structures of

Table 1
Crystallographic data of lysozyme crystals.

Z, No. of molecules in the unit cell. V_{solv}, (*v*/*v*) fraction of solvent in the crystal.

	Tetragonal	Orthorhombic	Monoclinic	Triclinic
Space group	$P4_32_12$	$P2_12_12_1$	$P2_1$	$P1$
Unit-cell parameters				
a (Å)	78.54	56.44	26.90	27.28
b (Å)	78.54	73.73	58.95	31.98
c (Å)	37.77	30.43	31.33	34.29
α (°)				88.53
β (°)			111.9	108.57
γ (°)				111.85
Z	8	4	2	1
V_{solv}	0.39	0.43	0.22	0.26

the four forms have been determined by single-crystal X-ray analysis (Vaney *et al.*, 1996; Berthou *et al.*, 1983; Madhusudan *et al.*, 1993; Hodsdon *et al.*, 1990). From the known crystal structures, it is possible to investigate the specificities of the intermolecular interactions constituted of hydrogen, ionic and van der Waals interactions. We have already analyzed the orthorhombic (Oki *et al.*, 1999) and monoclinic (Hondoh *et al.*, 2001) lysozyme crystals by estimating the macrobond strengths in the crystal. These macrobonds form periodic bond chains (PBC; Hartman, 1973) that control the overall morphology of the crystals (Durbin & Feher, 1991; Strom & Bennema, 1997*a*,*b*). Although the real force field of intermolecular interactions in protein crystals is considered to be highly complex, previous studies have shown that even the simplest estimation of macrobond strength leads to a reasonable correlation between the morphology and PBC of macrobonds. In this paper, we describe advanced features of the intermolecular contacts in protein crystals based on the four lysozyme crystal structures in order to obtain a better understanding of the nature of the contacts.

2. Procedures

2.1. Structure data

The coordinates of the atoms in lysozyme crystals were taken from the Protein Data Bank (PDB; Berman *et al.*, 2000) for tetragonal (PDB code 193l), orthorhombic (1bgi), monoclinic (1lma) and triclinic (2lzt) lysozyme. For the monoclinic crystal, we have chosen for simplicity the low-humidity form which contains one molecule in the asymmetric unit (Rao & Sundaralingam, 1996), instead of the as-grown crystal which contains two molecules in the asymmetric unit. This transition in the solid phase, which is accompanied by an ~10% loss of water content, does not cause much change in the packing of the molecules or in the crystal habit. Since the atomic coordinates of the bound waters in the low-humidity monoclinic and triclinic entries were not given for a compact unit of one molecule, the coordinates were reduced using symmetry to form one cluster of bonding units for use in the present study. The space groups and unit-cell parameters for these crystals are summarized in Table 1.

2.2. List of contacts

The program *DISMAP* (Fortran/MS-DOS on an NEC PC9821 personal computer) written by YM was used to list the intermolecular interatomic interaction pairs. This program first picks out two molecules in which at least one pair of polypeptide atoms lie within a distance of 4 Å, which defines the two molecules as being in contact. Every atom pair with a distance less than 4 Å is further listed for each contact site. These are classified into five non-covalent bonding categories: amino acid–amino acid, amino acid–water, water–water and heteroatom-involved hydrogen bonds, and other non-hydrogen-bond interactions which were regarded as van der Waals interactions (VDW). Hydrogen bonds were defined as pairs having a distance of less than 3.5 Å which were constituted of potential hydrogen-bonding atoms (Ippolito *et al.*, 1990). Since we do not know the positions of H atoms and the exact ionic character of the polar atoms, possible ionic bonds (or salt bridges) are included in the category of hydrogen bonds.

2.3. Calculation of bond strength

The individual atomic interaction pairs, even in the case of the same bond type, should have different bond strengths depending on the micro-environments in the structure of molecule. However, as in the previous study for an orthorhombic crystal (Oki *et al.*, 1999), we assumed a single value for a non-covalent bond as follows. The strength of a hydrogen bond, for a typical example of O—H···O, ranges from 21 to 10.5 kJ mol^{-1} depending on the bond distances (Jeffrey & Saenger, 1991), which are within the range 2.5–3.5 Å in protein molecules. Hydrogen bonds are formed mainly between O and N atoms. The electronegativity of nitrogen is smaller than that of oxygen and the strength of the hydrogen bond in this case would be smaller than that above. Thus, we adopted a value of 12.5 kJ mol^{-1} as a representative value for all hydrogen bonds. Possible salt bridges and ionic bonds are regarded as hydrogen bonds, although they may have higher binding energies. For water-assisted hydrogen bonds we used half the value, because the temperature factors (thermal vibration) of bound water molecules are generally higher than those of amino acids, suggesting that this hydrogen bond is weaker. For the strength of 'van der Waals' (VDW) contacts, not only dispersion forces but also those derived from permanent dipoles are included. To perform this, we used the Lennard–Jones potential parameters derived from viscosity data (Reid *et al.*, 1977), which show that the strength lies in the range 0.8–2.5 kJ mol^{-1} for non-polar compounds. However, in the present calculations the category of VDW contacts include those atomic pairs of distance up to 4 Å, which is longer than the usual VDW distance. Thus, a modest value of 1.3 kJ mol^{-1} was adopted. In summary, we assigned values of 12.6, 6.3, 2.9 and 1.3 kJ mol^{-1}, respectively, for amino acid–amino acid, amino acid–water and water–water hydrogen bonds, and other interaction pairs (VDW). Amino acid–ionic heteroatom (*e.g.* Cl^-) pairs were assigned a value equivalent to that of amino acid–amino acid hydrogen bonds. These assumptions,

Table 2
Equivalent positions of the molecules forming macrobonds.

In each macrobond, for example A of the orthorhombic form, site A in the molecule at (x, y, z) forms a contact with site A' in the molecule at $(x - \frac{1}{2}, -y + \frac{1}{2}, -z + 1)$; the site A' in the molecule at (x, y, z) forms a contact with the site A in the molecule at $(x + \frac{1}{2}, -y + \frac{1}{2}, -z + 1)$.

Tetragonal	
A: $(-y, -x, -z + \frac{1}{2})$	$A' = A$ (twofold axis related)
B: $(y, x, -z + 1)$	$B' = B$ (twofold axis related)
C: $(y - \frac{1}{2}, -x + \frac{1}{2}, z + \frac{1}{4})$	C': $(-y + \frac{1}{2}, x + \frac{1}{2}, z - \frac{1}{4})$
D: $(-y + \frac{1}{2}, x + \frac{1}{2}, z + \frac{3}{4})$	D': $(y - \frac{1}{2}, -x + \frac{1}{2}, z - \frac{3}{4})$
Orthorhombic	
A: $(x - \frac{1}{2}, -y + \frac{1}{2}, -z + 1)$	A': $(x + \frac{1}{2}, -y + \frac{1}{2}, -z + 1)$
B: $(x, y, z - 1)$	B': $(x, y, z + 1)$
C: $(-x + \frac{1}{2}, -y + 1, z - \frac{1}{2})$	C': $(-x + \frac{1}{2}, -y + 1, z + \frac{1}{2})$
Monoclinic	
A: $(x - 1, y, z - 1)$	A': $(x + 1, y, z + 1)$
B: $(x - 1, y, z)$	B': $(x + 1, y, z)$
C: $(x, y, z - 1)$	C': $(x, y, z + 1)$
D: $(-x + 1, y - \frac{1}{2}, -z + 1)$	D': $(-x + 1, y + \frac{1}{2}, -z + 1)$
Triclinic	
A: $(x - 1, y - 1, z)$	A': $(x + 1, y + 1, z)$
B: $(x - 1, y, z - 1)$	B': $(x + 1, y, z + 1)$
C: $(x - 1, y, z)$	C': $(x + 1, y, z)$
D: $(x, y - 1, z)$	D': $(x, y + 1, z)$
E: $(x, y - 1, z + 1)$	E': $(x, y + 1, z - 1)$
F: $(x, y, z - 1)$	F': $(x, y, z + 1)$

although arbitrary to some extent, are aimed as making a first-cut theoretical estimation to serve as a viability test for comparison with experiments and further adjustment. It is difficult to present the absolute quantitative error associated with these estimates. However, since the estimation is made using the same assumptions for all crystals and further because of the averaging of the individualities in each type of interaction in a contact, the error in the relative strength should be sufficiently small for use in the present discussion. The macrobond strengths were calculated as the sum of the strengths of the bonds which make up a contact site.

2.4. Coulombic interaction within a contact

In addition to the above aspects of the contacts, Coulombic interaction forces were calculated for every interacting pair of atoms other than those forming a hydrogen bond. The partial charges for the atoms of amino-acid residues were taken from the AMBER force field (Cornell *et al.*, 1995). The partial charges q (in units of e^-) were assigned to the chemical groups, including attached H atoms. Values for the main-chain atoms of glycine are (where q is given in parentheses): C^α (0.045) = C (−0.025) + H (0.070), NH (−0.144) = N (−0.416) + H (0.272), C (0.597) and O (−0.568). For side-chain atoms, for example for aspartic acid, CH_2 (−0.054) = C^β (−0.030) + H (−0.012) × 2, C (0.799) and two O (−0.801); for alanine, CH_3 (−0.003) = C^β (−0.183) + H (0.060) × 3. The q value for the O atom of bound water was assigned a value of −0.6. The sum of $q_i q_j$ for all interaction pairs of distance less than 4 Å, except for the hydrogen bonds, was calculated for each macrobond site.

2.5. Surface area of contact

To estimate the contact surface area of the molecules in a macrobond, the exposed surface areas of the atoms in the free molecule were calculated using a computer program composed according to the method described by Richards (1977). The accessible surface area (ASA) of an atom is defined as the area of locus of the centre of a probe (water molecule) which is in contact with the van der Waals surface of the atom. This gives a reasonable estimate of the surface area that is hydrated upon dissolution. We obtained the ASA values for every atom in the molecule, including bond-assisting water molecules and heteroatoms. The definition of the surface area of contact between two molecules is not straightforward, since the molecular surface is atomically rough. However, we defined the molecular surface area which is buried in a contact as the sum of the ASA values of the atoms involved in a macrobond. These calculations give two slightly different values for two molecules in contact.

2.6. Polar-coordinate representation of contact

To show the location of macrobonds on the surface of the molecule, we devised a polar-coordinate representation as follows. The coordinates of the atoms as taken from the PDB are normally represented with reference to orthogonal crystal axes. To compare the positions of the contacts on the molecular surface in different polymorphic modifications, the crystal coordinates were transformed to molecular coordinates. The axes of the molecular coordinates were chosen orthogonally, with the origin at the centre of the molecule, the X axis in reference to an arbitrarily chosen point, Y in reference to a second point and Z forming a right-handed set of axes with X and Y. The points of reference were chosen as the averaged coordinates of ten C^α atoms for each polymorph in order to eliminate relative coordinate errors between the polymorphs. The molecular coordinates were then transformed to the polar coordinates (r, θ, φ) for any contact point under consideration on the molecular surface, where r is the distance from the origin to this point, θ (0 to 180°) is the angle from the Z axis and φ (−180 to 180°) is the angle from the $-X$ axis in the plane XY. The angular coordinates (θ, φ) were plotted graphically using a PostScript interpreter with a Tektronix Phaser printer connected to the computer described in §2.2.

3. Results

3.1. Macrobond composition and strength

The analysis showed that each molecule in the four crystal polymorphs has six, six, eight and 12 molecules in contact for the tetragonal, orthorhombic, monoclinic and triclinic modifications, respectively. The equivalent crystallographic positions of the molecules in contact with the molecule at (x, y, z) are shown in Table 2. In this table, the primed and unprimed sites are the counterparts in the contact. To supplement this table, a schematic representation of the macrobonds connecting equivalent molecules in the crystal lattice is shown

in Fig. 1. In the *A* and *B* sites of the tetragonal crystal, the contact is formed between molecules related by the twofold axis, which therefore face each other with the same surfaces of opposing polarity. Selected hydrogen-bonded (or salt-bridged) atom pairs in each macrobond site are listed in Table 3. The total numbers of interacting pairs and the calculated strengths of the macrobonds are listed in Table 4. The strength of a macrobond is calculated as the sum of the contributions of the bond energies of the different types listed. As shown in this table, the number of non-H atom interaction pairs (VDW) is about three times greater than the sum of the hydrogen bonds. The number of direct amino acid–amino acid hydrogen bonds is less than the number of water-mediated contacts. However, the direct hydrogen bonds and those involving heteroatoms are considered to be specific for the protein molecules and solute species, making an indispensable contribution to the formation of a contact in a crystal. The

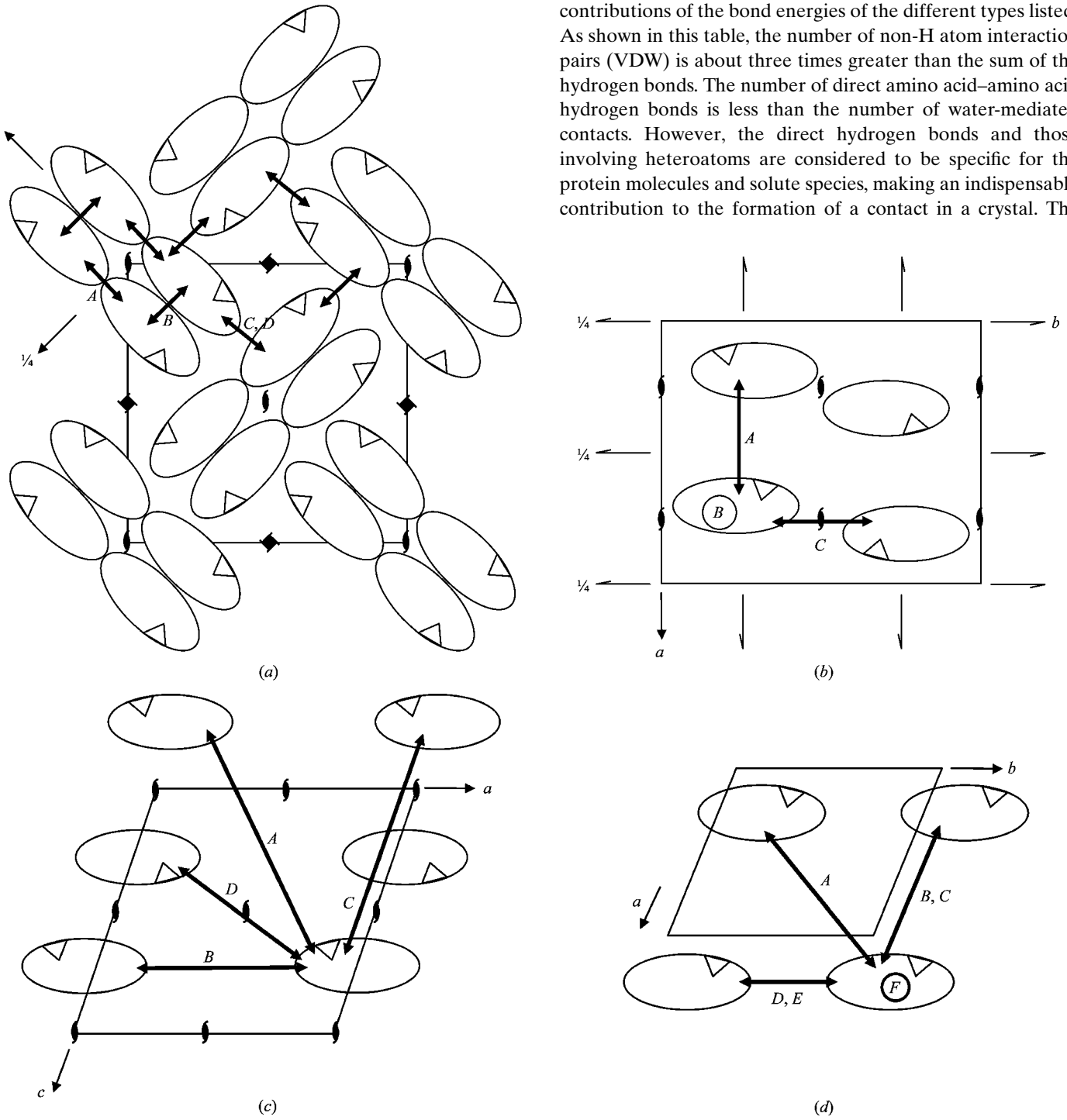

Figure 1
Schematic representation of the macrobonds (arrows) connecting equivalent molecules in the four crystal modifications: (*a*) tetragonal, (*b*) orthorhombic, (*c*) monoclinic and (*d*) triclinic, projected along the *c* axis except for the monoclinic form (*b* axis). Symmetry elements are indicated according to the International Tables for X-ray Crystallography. The shape of the molecule is drawn schematically and smaller than the real one for clarity. Macrobonds are labelled corresponding to Table 2. The circled macrobonds *B* in the orthorhombic and *F* in the triclinic forms connect molecules lying parallel along the *c* axis. The macrobonds *C* and *D* in the tetragonal form are superposed in the projection, respectively running left- and right-handed helically along the 4_3 axis. The macrobonds *B* and *D* in the triclinic form are superposed with *C* and *E*, respectively, connecting the molecules separated by one lattice unit along the *c* axis.

heteroatoms are chloride ions in the tetragonal and orthorhombic forms and nitrate ions in the monoclinic and triclinic forms, which are incorporated from the crystallization solution.

Table 3
Selected hydrogen-bonded atom pairs in the macrobonds of the four crystal modifications.

In each atom pair, the first atom belongs to the unprimed macrobond site and the second to the primed site.

Tetragonal†	
A	Lys13 N^{ζ}—Oxt129; Arg14 O—Arg128 $N^{\eta 2}$
B	Asn39 $N^{\delta 2}$—Asp66 O; Gln41 $O^{\varepsilon 1}$—Ser81 N; Gln41 $N^{\varepsilon 2}$—Asn65 O; Thr43 O—Arg68 $N^{\eta 1}$
C	Gly22 O—Arg114 $N^{\eta 1}$; Asn106 $N^{\delta 2}$—Asn113 O; Cl^-—Asn113 $N^{\delta 2}$
D	Thr47 $O^{\gamma 1}$—Gly126 O
Orthorhombic	
A	Asn113 O—Ser85 O^{γ}; Asp119 O—Ser81 O^{γ}; Arg125 $N^{\eta 1}$—Asn65 O; Arg125 $N^{\eta 1,2}$—Cl^-
B	Gln41 $O^{\varepsilon 1}$—Arg21 $N^{\eta 1}$; Arg45 N^{ε}—Gly102 O
C	Arg61 $N^{\eta 1,2}$—Gly102 O
Monoclinic	
A	Asn113 O —Ser81 O^{γ}; Lys116 N^{ζ}—Asn77 $O^{\delta 1}$
B	Arg114 $N^{\eta 1}$—Gly16 O; Arg114 $N^{\eta 2}$—Asp18 O
C	Asn19 $N^{\delta 2}$—Gln41 $N^{\varepsilon 2}$; Arg21 O—Arg68 $N^{\eta 2}$
D	Arg61 N^{ε}—Asp119 $O^{\delta 2}$; Arg61 $N^{\eta 2}$—Asp119 $O^{\delta 1}$; Arg112 $N^{\eta 2}$—Cys6 S^{γ}
Triclinic	
A	Asn77 $O^{\delta 1}$—Lys116 N^{ζ}; NO_3^-—Lys116 N^{ζ}
B	Arg14 $N^{\eta 2}$—Asp48 $O^{\delta 2}$
C	Gly16 O—Arg114 $N^{\eta 1}$; Asn77 $N^{\delta 2}$—Arg45 O
D	Asp66 O—Arg21 $N^{\eta 2}$: Ser81 O—Asn19 $N^{\delta 2}$
E	Gly67 O—Gly126 N
F	Glu7 $O^{\varepsilon 2}$—Asp101 $O^{\delta 2}$; Arg128 $N^{\eta 2}$—Ser100 O^{γ}; NO_3^-—Arg73 $N^{\eta 2}$

† In tetragonal *A* and *B*, the pairs of atoms appear twice in a macrobond owing to the twofold axis symmetry relation.

3.2. Coulombic interaction

The sums of q_iq_j for each macrobond site are listed in Table 5, where the summation is only taken over the VDW interaction pairs. Potential hydrogen-bond pairs were not considered in this calculation, since they consist of polar atoms with an H atom in between them stabilizing the bond. Without considering the H atom, the simple product of the charges will result in an apparent false repulsive force. Table 5 shows that the sum of q_iq_j is negative in every macrobond site, except for a small positive sum in site *A* of the monoclinic polymorph. These results suggests that the macrobond is essentially formed by attractive electrostatic forces making up the background of the contact. The energy values derived from these Coulombic forces are given in parentheses in this table in kJ mol^{-1}. This energy is calculated as $\sum q_iq_j/(\varepsilon d_{ij})$, with the average distance d_{ij} and a dielectric constant ε of 20, using $e = 1.6 \times 10^{-19}$ C (4.8×10^{-10} esu), with the actual charges being qe. The average distance for VDW interaction pairs was calculated to be close to 3.7 Å in every site and was used for calculation. The value of dielectric constant on the surface of the molecule has been a matter of great dispute. Here, we have chosen a value of 20, which has been shown to agree as a whole with the experimental results (Antosiewicz *et al.*, 1994). By calculation using these parameters, the Coulombic energies are shown to exhibit smaller values than those of corresponding VDW interaction energies, as compared with those in the 'other interactions' column in Table 4.

Table 4
Summary of macrobond parameters in lysozyme crystals.

		Hydrogen bonds†							
Macrobond	Total No. of interactions‡	Amino acid–amino acid	Amino acid–water	Water–water	Chloride or nitrate involved	Other interactions†	Macrobond strength E_b (kJ mol^{-1})	Surface area S_b§ (Å^2)	Energy density¶ (10^{-3} J m^{-2})
Tetragonal									
A	121	12 (151)	10 (63)	9 (26)	0	84 (105)	345	904	64
B	183	16 (201)	12 (75)	26 (76)	0	119 (149)	502	1230	68
C, *C*′	123	6 (75)	12 (75)	1 (38)	1 (12)	79 (99)	299	666, 671	74
D, *D*′	28	1 (13)	3 (19)	1 (3)	0	23 (29)	63	257, 365	34
Orthorhombic									
A, *A*′	108	4 (50)	15 (94)	6 (18)	1 (12)	79 (103)	271	741, 697	63
B, *B*′	69	4 (50)	5 (31)	4 (12)	0	51 (64)	157	476, 539	52
C, *C*′	50	3 (38)	8 (50)	1 (3)	0	38 (48)	138	533, 390	50
Monoclinic									
A, *A*′	56	2 (25)	5 (31)	3 (9)	0	45 (56)	122	480, 472	43
B, *B*′	57	3 (38)	6 (38)	1 (3)	0	44 (55)	133	634, 536	38
C, *C*′	99	7 (88)	15 (94)	4 (12)	0	71 (89)	283	956, 838	53
D, *D*′	159	3 (38)	13 (82)	16 (47)	5 (63)	114 (143)	373	1102, 1012	59
Triclinic									
A, *A*′	66	4 (50)	6 (38)	4 (12)	1 (13)	48 (60)	173	608, 527	51
B, *B*′	38	0	4 (25)	2 (6)	0	31 (39)	70	492, 514	23
C, *C*′	88	4 (50)	10 (63)	16 (48)	0	48 (60)	221	755, 793	48
D, *D*′	81	6 (75)	5 (31)	8 (23)	1 (13)	56 (70)	212	603, 616	58
E, *E*′	17	1 (12)	0	1 (3)	0	14 (18)	33	223, 220	25
F, *F*′	99	7 (88)	11 (69)	9 (26)	1 (13)	66 (83)	279	713, 703	66

† The estimated energy (kJ mol^{-1}) is given in parentheses. Chloride-involved bonds are found in the tetragonal and orthorhombic forms, nitrate-involved bonds are found in the monoclinic and triclinic forms. ‡ The sum of the numbers of bonds does not necessary agree with the total number of interactions, owing to exclusion of water–water pairs of $d > 3.5$ Å and N–N pairs of $d < 3.5$ Å. § Surface area calculated as in text. ¶ Energy density is given by the macrobond strength divided by the average surface area.

Table 5
Coulombic interaction of macrobonds in lysozyme crystals.

	$\sum q_i q_j$†‡
Tetragonal	
A	−4.7 (88)
B	−5.9 (110)
C, *C*′	−3.1 (58)
D, *D*′	−0.9 (17)
Orthorhombic	
A, *A*′	−3.0 (56)
B, *B*′	−1.3 (24)
C, *C*′	−1.3 (24)
Monoclinic	
A, *A*′	0.1 (−2)
B, *B*′	−1.5 (28)
C, *C*′	−4.3 (80)
D, *D*′	−3.4 (64)
Triclinic	
A, *A*′	−1.1 (21)
B, *B*′	−0.4 (7)
C, *C*′	−1.4 (26)
D, *D*′	−3.2 (60)
E, *E*′	−0.4 (7)
F, *F*′	−4.8 (90)

† $\sum q_i q_j$ is given in units of e^2. ‡ The values in parentheses are the Coulombic interaction energy (kJ mol^{-1}) calculated using $e = 4.8 \times 10^{-10}$ esu, an average dielectric constant of 20 and a distance of 3.7 Å.

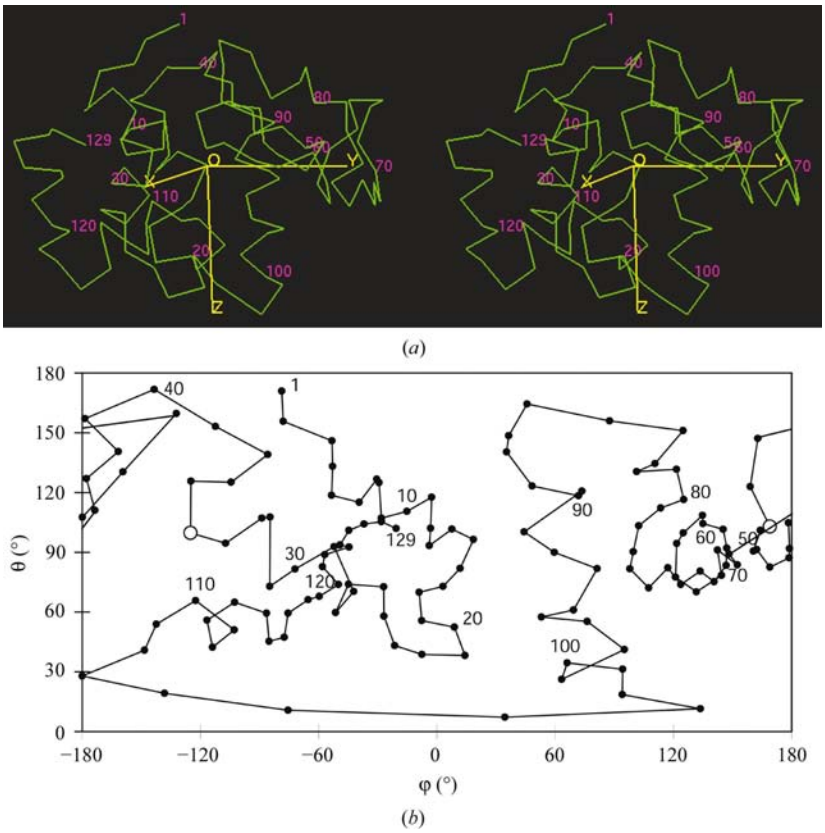

Figure 2
A stereoscopic drawing of the C^{α}-atom chain of a lysozyme molecule with molecular-coordinate axes. Residue numbers are shown every ten atoms. A Mercator plot of the positions of C^{α} atoms corresponding to those in (*a*). The active-site atoms Glu35 C^{α} and Asp52 C^{α} are indicated as open circles. The approximate positions of the macrobonds can be placed by comparing these figures with Table 3, locating a specific residue on this map and thus in Fig. 3. The molecular-coordinate axes *X*, *Y* and *Z* correspond to (φ, θ) values of $(0, 90^{\circ})$, $(90, 90^{\circ})$ and $(-90, 0^{\circ})$ (since φ cannot be defined at $\theta = 0^{\circ}$), respectively, with the origin at the centre of the molecule. The regions of θ near 0° and 180° appear extended along φ owing to the character of the Mercator projection.

3.3. Surface area of contact

The contact areas (S_b) for each macrobond site are also shown in Table 4. In each macrobond site, except for those between molecules related by a twofold axis, primed and unprimed sites have different values, as described in §2.5. In the present study, the averaged contact surface area for the two molecules in contact will be used as the surface area of contact. The total contact surface areas in the four polymorphs are 4093, 3376, 6030 and 6767 Å^2 and the ratios of these values to the total surface area of free molecule (7255 Å^2 on average) are 0.58, 0.49, 0.79 and 0.91 for the tetragonal, orthorhombic, monoclinic and triclinic polymorphs, respectively.

3.4. Polar-coordinate representation

The graphical definition of polar coordinates is given in Fig. 2, showing a stereoscopic picture of a C^{α} molecule of lysozyme as well as the molecular coordinate axes and a plot of all C^{α} positions in the polar-coordinate system. On the basis of these definition, the contact points at every macrobond site have been plotted in polar coordinates as shown in Fig. 3, summarizing the plots for each crystal system represented by the Mercator projection. The water-mediated hydrogen bonds are also included. These figures show how the surface of the molecule is covered by the contact molecules as viewed from the centre of the molecule.

4. Discussion

4.1. Features of macrobonds

PBC studies have been conducted concerning the crystal-growth features of the tetragonal modification (Nadarajah & Pusey, 1996; Strom & Bennema, 1997*a*,*b*). In tetragonal lysozyme, the macrobonds *A* and *B*, which possess the two highest strengths, as shown in Table 4, are formed by two mutually but not directly crossing twofold axes normal to the *c* axis (Fig. 1*a*). Furthermore, they connect the molecules along the twofold screw axis *via* one PBC composed of alternating macrobonds *A* and *B*. In contrast, the macrobonds *C* and *D* connect the molecules along the fourfold screw axis *via* two independent PBCs each composed of pure *C* and *D*. The macrobonds *X*, *Y* and *Z* (Monaco & Rosenberger, 1993) correspond to *A*, *B* and *C* in the present paper and there is another weaker macrobond *D*. One even weaker bond reported previously (Nadarajah & Pusey, 1996), which connects the molecules separated by a unit-cell length along the *c* axis *via* only one water-mediated hydrogen bond, was excluded from the contact by our

definition. An estimate of the relative strength of the macrobonds in the tetragonal form, X:Y:Z = 2:4:5, was previously suggested from a Monte Carlo simulation based on a simple model (Durbin & Feher, 1991). The discrepancies between the present results (7:10:6) may arise from the geometrical model used and the neglection of macrobond D, as well as the method employed.

For the orthorhombic crystal, macrobond analysis has previously been reported (Oki *et al.*, 1999) and shows a reasonable agreement between the morphology and the structure. The analysis for the as-grown monoclinic crystal has also shown good agreement (Hondoh *et al.*, 2001). The largest number of contacts (12) in the four polymorphs exists in the triclinic crystal. Since only pure translational symmetry exists in the triclinic system, this fact suggests that only pure crystallographic translational operations can find stable intermolecular contacts. It was also shown that several pairs of molecules in contact exist that have the same relative orientation but differ only in translational parameters among the different modifications. Such examples are found among pairs of molecules in contact between (x, y, z) and $(x, y - 1, z)$ in macrobond D of the triclinic form, $(x - 1, y, z)$ in B of the monoclinic form and $(x, y, z - 1)$ in B of the orthorhombic form. In the triclinic modification, five nitrate ions are involved, suggesting the importance of these ions in establishing firm contacts. The ratios of the contact surface to the whole surface given in §3.3 may also be reflected by the resolution of the X-ray diffraction, so that the larger the ratio the higher the resolution, as roughly implied in the resolutions used in the analyses of the crystal structures: 1.33 Å for PDB code 193l collected using synchrotron radiation, but more generally 1.7–2.0 Å for the tetragonal form (Vaney *et al.*, 1996), 1.7 Å for the orthorhombic form, 1.75 Å for the monoclinic form and 1.5 Å for the triclinic form.

4.2. Macrobonds and hydration

The total work required to completely dissociate a crystal into separated single molecules in vacuum ($\Delta H_{\rm macro}$) is the lattice energy of the crystal. This evaporation process requires the rupture of all macrobonds between molecules. The total macrobond strengths in the crystals of the four polymorphs are 1209, 566, 911 and 988 kJ mol^{-1}, respectively, for the forms in Table 4. Dissolution of the crystal in a solvent within which the separated molecules do not interact, may be accomplished by first separating the molecules in vacuum and then placing them into the solvent, retrieving the hydration enthalpy, $\Delta H_{\rm hyd}$. As a result, the approximate relation $\Delta H_{\rm macro} = \Delta H_{\rm hyd} + \Delta H_{\rm dis}$ holds (Hondoh *et al.*, 2001), where $\Delta H_{\rm dis}$ is the dissolution enthalpy. The dissolution enthalpies obtained from the solubility measurements in typical crystallization solutions are 70–110, 34, 102 and 155 (above 298 K) and 56 (below

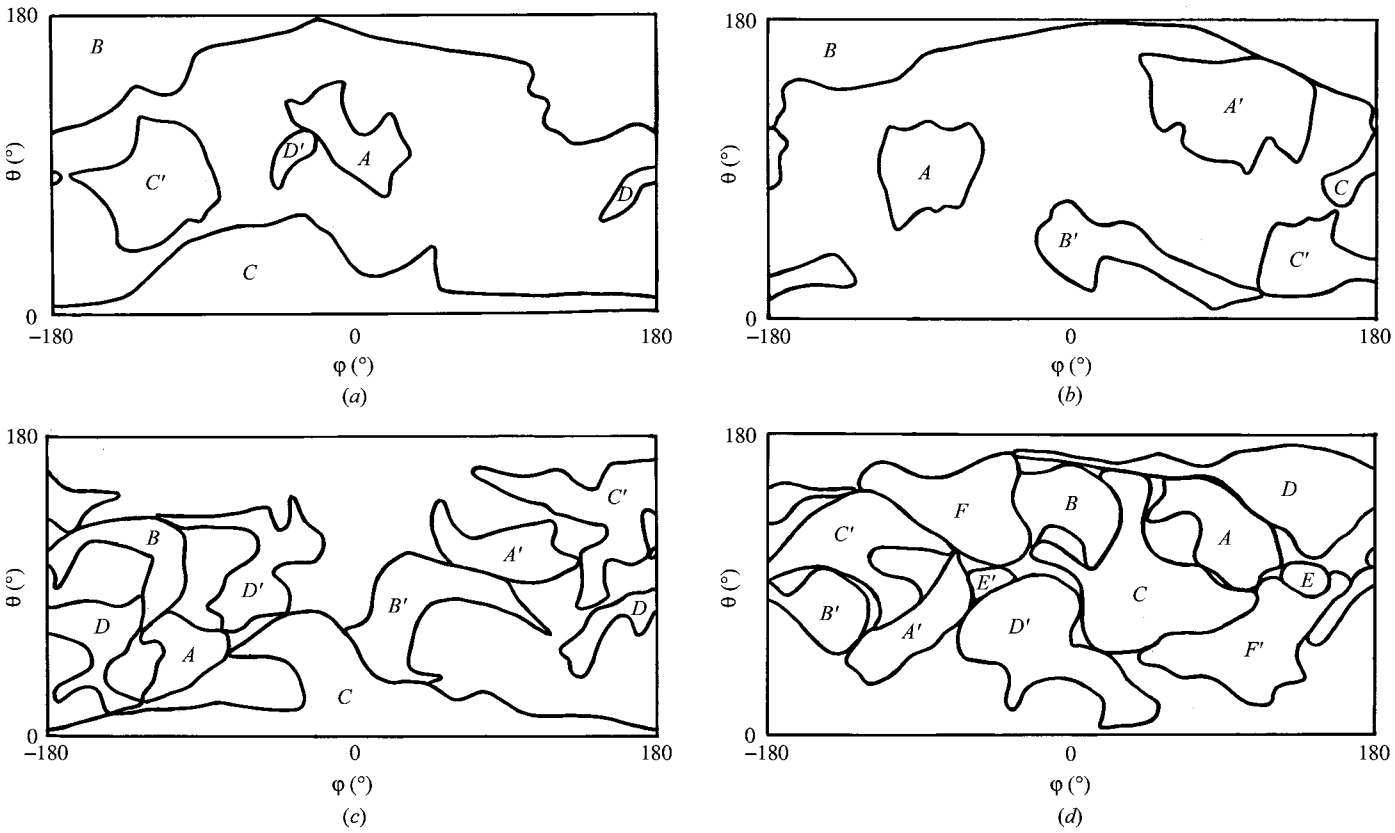

Figure 3
Distribution of the areas of molecular surface covered with the macrobonds in lysozyme crystals of (*a*) tetragonal, (*b*) orthorhombic, (*c*) monoclinic and (*d*) triclinic forms, expressed in polar coordinates. The names of the macrobonds in each crystal system are indicated in the enclosures. The polar coordinates are defined as in Fig. 2.

298 K) kJ mol^{-1} for the tetragonal (Ataka & Asai, 1988; Rosenberger *et al.*, 1993; Sazaki *et al.*, 1999), orthorhombic (Ataka & Asai, 1988; Sazaki *et al.*, 1999), monoclinic (Hondoh *et al.*, 2001) and triclinic (Hondoh, Sazaki & Matsuura, unpublished results) forms, respectively. The ratio $\Delta H_{\rm dis}/\Delta H_{\rm macro} = \chi$ is equal to 5.8–9.1, 6.0, 11 and 15 (5.7) $\times 10^{-2}$, respectively, for these crystals. The similar figures for χ may be interpreted as a consequence of the similar composition of the ionic/atomic groups involved in every contact and also because hydration may take place in an approximately uniform manner independent of crystal packing. Still, one reason for the difference between crystals may be associated with the entropic contribution to $\Delta H_{\rm dis}$ both from the macromolecule and the water molecules. The difference might also be correlated with the variation of the solution composition and the solvent content ($V_{\rm solv}$ in Table 1). The proximity of χ and its small value, $\sim$0.1, suggests that the hydration energy $\Delta H_{\rm hyd}$ is roughly proportional to the total area of contact and is close to the magnitude of intermolecular bond strength. The factor $1 - \chi$ is essentially a measure of the hydrophilicity: a value of unity means complete wetting of the molecule by the solution. The contribution of bound water molecules may also be important. It is shown in the present analysis that the magnitude of the total strength of water-mediated bonds is comparable to that of amino acid–amino acid hydrogen bonds (Table 4).

Table 6
Macrobond strengths and surface energies.

$V_{\rm across}$ and $E_{\rm across}$ are the macrobond component and the energy which crosses this face, respectively. $\gamma_{\rm vac}$ and $\gamma_{\rm hyd}$ are the surface energy in vacuum and in the hydrated state, respectively.

Face	$V_{\rm across}$	$E_{\rm across}$ (kJ mol^{-1})	$S(hkl)$ (Å^2)	$\gamma_{\rm vac}$ (10^{-3} J m^{-2})	$\gamma_{\rm hyd}$ (10^{-3} J m^{-2})
Tetragonal					
(100)	$A + B + 2C + 2D$	3265	2998	43.5	12.3
(001)	$2A + 2C + 6D$	1666	6257	22.1	9.6
(110)†	$2A + 2B$	1694	4240	33.2	7.9
(101)†	$2A + 2C + 6D$	1666	6938	20.0	8.7
Orthorhombic					
(100)	$2A$	542	2244	20.1	5.6
(010)†	$2C$	276	1717	13.4	7.2
(001)	$4B + 2C$	904	4161	18.1	8.9
(011)†	$4B + 2C$	904	4501	16.8	8.2
(101)	$2A + 4B + 2C$	1446	4727	25.6	10.3
(110)†	$2A$	542	2825	16.0	4.4
Monoclinic‡					
(100)†	$2A + 2B$	510	1847	22.9	19.1
(010)†	D	373	781	39.6	13.1
(001)†	$2A + 2C$	810	1587	42.3	22.6
(10$\bar{1}$)†	$2B + 2C$	832	1934	35.7	10.7
(101)	$2A + 2B + 2C + 2D$	1822	2848	53.1	26.9
(110)	$2A + 2B + D$	883	1446	50.7	31.5
(011)	$2A + 2C + D$	1183	1770	55.5	26.0

† Developed crystallographic face. Morphologies are described in the references cited in the text. ‡ In the present low-humidity monoclinic crystal, the crystallographic axes were transformed from those in the as-grown monoclinic crystal (Hondoh *et al.*, 2001), such that $c' = (a - c)/2$, changing the index (101) to (100).

4.3. Surface energy

Estimation of the energy of macrobonds crossing a certain crystallographic plane enables us to evaluate the crystal vacuum specific surface energy for this face. To take hydration into account, we employed an estimation of the interfacial energy between two phases, protein crystal face and water, using the surface energies of these two phases in vacuum as described later.

From the macrobond strengths (E_b) for the polymorphs of lysozyme crystal shown in Table 4 and the macrobond components crossing each face, we analyzed the PBC in a similar way as in the previous study for the orthorhombic modification (Oki *et al.*, 1999). The results for tetragonal, orthorhombic and monoclinic crystals are shown in Table 6. Here, $V_{\rm across}$ is the macrobond component which crosses each crystallographic face and $E_{\rm across}$ is the calculated total macrobond strength crossing the face. The $S(hkl)$ (the unit-cell areas on each crystal face) and the surface energies calculated as described below are also shown. The surface energies in vacuum were estimated by simply dividing $E_{\rm across}$ by the area per unit cell; that is, $\gamma_{\rm vac} = E_{\rm across}/2S(hkl)$. As shown in this table, they are close to the magnitudes for common organic compounds (Israelashvili, 1992), but differ greatly from those ($\sim 10^{-3}$ J m^{-2}) estimated for protein crystal–solution interfaces found from crystal nucleation and growth experiments (Malkin & McPherson, 1994; Chernov, 1997). The difference should arise from hydration in the first place. Debye screening by solute ions also reduces surface energy. As shown in Table 6, in each polymorph the values of $\gamma_{\rm vac}$ are the smallest for the morphologically developed faces. In the tetragonal crystal form, the value for (110) does not fit this sequence, but it is smaller than that of (100), indicating that (110) is morphologically more important than (100). These facts suggest that even the surface energies estimated in vacuum reflect the morphology, which may be interpreted as showing that the hydration layer is, on average, similar for different crystal faces, so that major contributions to crystallographic anisotropy come from the crystal structure.

The hydration of the crystal surfaces may be taken into account as follows. The binding energy between two different materials (protein crystal face and water) is often approximated as the geometrical mean between the binding energies within each of the materials (Israelashvili, 1992). The energy $2\gamma_W S_b$ is released when water is cut and separated along the surface S_b, *i.e.* two water–vacuum interfaces of total area $2S_b$ are created, $\gamma_W = 7.3 \times 10^{-2}$ J m^{-2} being the surface tension of pure water. Therefore, the energy per hydrated bond is

$$\varepsilon_b = [E_b^{1/2} - (2\gamma_W S_b)^{1/2}]^2. \quad (1)$$

The contact surface areas (S_b) of macrobonds are listed in Table 4. The hydrated macrobond strength $\varepsilon_{\rm across} = \sum n_b \varepsilon_b$, where n_b is the number of macrobond components ($V_{\rm across}$) listed in Table 6. By using the same equation as above, the interfacial surface energy with due account for hydration is given by $\gamma_{\rm hyd} = \varepsilon_{\rm across}/2S(hkl)$. The calculated values are also given in Table 6.

Since the obtained values for the 'dangling-bond' energies ε_b are small differences between larger numbers, the accuracy of the estimate given above should not be high. Nevertheless,

the hierarchy of the crystal face energies correctly describes the development of the corresponding faces on the crystal habit. This hierarchy is close, but not identical, to that following the crystal–vacuum surface energies. The proximity of the hierarchies follows naturally from the fact that anisotropy only arises from the crystal. The difference may be understood in terms of the different densities of various atomic bonds within different contacts and correspondingly to different hydration energies. In comparison with the observed crystal habit, it should not be forgotten that this habit is the growth rather than the equilibrium shape of the crystal.

Equally important, the absolute surface energies vary from several to $\sim 30 \times 10^{-3}$ J m^{-2}. These figures are, of course, several times lower than $\gamma_{\rm vac}$, but still exceed the experimentally found surface energy for tetragonal lysozyme ($\sim 1 \times 10^{-3}$ J m^{-2}; Chernov, 1997). The larger absolute figures for crystal–solution surface energies come from noticeably larger figures for the term $(2\gamma_W S_b)^{1/2}$ in (1). As shown in our calculation process, in all macrobond sites of all polymorphs concerned, this term is always 1.5–2.0 times larger than the first term. The probable cause may be inaccuracy of the surface area per contact or deviation of γ_W from that of pure water owing to the solutes in the solvent. More importantly, Debye screening of polar groups within the future contact patches by small ions in solution was not taken into account in these estimates. This screening, of course, diminishes the surface energy.

It follows from (1) that at some macrobond strengths and contact areas, the excess surface bond energy, *i.e.* the 'dangling-bond' energy, at the crystal–solution interface, ε_b, may vanish or at least become noticeably lower than the thermal energy kT. This may happen with several bonds, including those crossing steps of various azimuthal orientations on a given face. For such specific composition of solution and temperature, thermal fluctuations become strong compared with the dangling bonds tangential to the face under consideration. In this case, the configurational entropy is no longer negligible and a roughening transition should occur. For the orthorhombic case, $\varepsilon_A = 1.25 \times 10^{-19}$, $\varepsilon_B = 1.22 \times 10^{-19}$ and $\varepsilon_C = 1.17 \times 10^{-19}$ J, while $kT = 4.04 \times 10^{-21}$ J. Thus, all the considered faces should stay smooth, in agreement with the experiment. However, the proximity between the dangling-bond energies on the crystal–vacuum and solution–vacuum interfaces, $E_{\rm across}$ and $2\gamma_w S_b$, respectively, makes the roughening transition possible for some solution concentrations and temperatures. Indeed, some protein crystals have rounded surfaces in all or some ranges of crystallographic directions. This means that the corresponding interfaces with solution are disordered and grow not layer by layer but by addition of new molecules at all positions on the surface.

4.4. Coulombic contribution

As shown in Table 5, every macrobond site in every crystal exhibits attractive Coulombic interaction as a whole, although the individual contributions of atom pairs have small positive or negative values. This result seems to be quite natural, but it is still very interesting in that the calculation showed the contact force to be essentially electrostatically attractive. The same calculation in the present study also showed similar results (data not shown) for the polymorphous crystals of thaumatin (Ko *et al.*, 1994). These facts suggest that an intermolecular contact is formed by finding an electrostatically attractive position on the surface of the other molecule and then forming possible hydrogen bonds by adjusting toward more stable contacts, adapting to the force field of crystal lattice. A rational calculation of electrostatic interactions on macromolecular complex formation has been demonstrated using a computer simulation (Gilson & Honig, 1988).

Table 7
Strength of association in enzyme inhibitors evaluated analogous to macrobonding.

Complex	$E_{\rm assoc}$ (kJ mol^{-1})	$\sum q_i q_j$ (e^2)
Trypsin–BPTI	584	−7.6
Barnase–barstar	866	−10.4

In the present study, on reducing $\sum q_i q_j$ to the electrostatic energy we needed to know the value of the dielectric constant ε. This value could not be known exactly in the protein molecule, since it is highly dependent on the micro-environment in the protein structure and is also affected by the presence of disordered water, whose features are obscured. It is known to have a value of around 3 on the inside of a protein molecule and of around 80 in fully disordered water. We assumed a value of 20, which has been shown to be a reasonable value for the surface of the molecule (Antosiewicz *et al.*, 1994). This resulted in the calculated energy values shown in Table 5. The average value of the Coulombic energy is shown to be about half the magnitude of the corresponding VDW interaction energy. When we consider that these two energies originate from essentially the same intermolecular interactions, this result might suggest that the value of the global dielectric constant should be about 10, or that the VDW energy per interaction should be one half of the value 1.3 kJ mol^{-1}. The presence of disordered water in the crystal may also significantly affect the forces described above.

4.5. Features of polar plot

A plot of contacts using polar coordinates in reference to the molecular coordinates enables revelation of how the contact patches for various polymorphs are distributed over the molecular surface (Fig. 3). The enclosed area corresponds to the surface area of contact. The fractions of the molecular surface area occupied by contact patches are more than half, as described in §3.3, with an extremely high value in the triclinic modification. When the polar plots of the four polymorphs of lysozyme are superimposed, it becomes clear that almost any place on the surface of the molecule is involved in one or another contact in one of the four crystals, with the exception of the inside of the active site because of its concave geometry. This is an interesting feature of probably many protein crystals that demonstrate polymorphism. Thus, we

could say that probably almost any area on the surface of a protein molecule is capable of forming an intermolecular contact depending on the crystal-producing crystallization conditions, such as precipitant salts, PEG, other solutes, pH and temperature. One may thus say that screening for crystallization conditions is a process that produces, by changing the solution composition, an appropriate system of patches to acquire sufficient affinity to bind to one another and form a crystal. If the contrast difference between competing systems of patches is strong, one may expect well ordered crystals, especially at low or moderate supersaturations. Lack of contrast may result in orientationally or even translationally disordered crystals or just aggregates.

4.6. Comparison of macrobond strengths with other protein interaction systems

To evaluate the actual magnitude of the strength of the macrobonds in the crystal, we compared their strength of association with those in other protein–protein interaction systems, calculated in a similar way as described in §§2.3 and 2.4 (Tables 4 and 5). For this purpose, we have chosen two such protein–protein complexes, trypsin–BPTI (Huber *et al.*, 1974; Vincent & Lazdunski, 1972) and barnase–barstar (Lee & Tidor, 2001; Buckle *et al.*, 1994). The dissociation constants (K_d) for these complexes are experimentally given as 6×10^{-14} and 1.3×10^{-14} M, which correspond to association energies of 76 and 80 kJ mol^{-1}, respectively. These are examples of extremely high association constants. The calculated values ($E_{\rm assoc}$) analogous to the macrobond strengths for these complexes are shown in Table 7. These values are three to four times higher than those of the macrobonds in crystals. The Coulombic interactions ($\sum q_i q_j$) also show similar ratios of strength. If we take the averaged ratio of the experimental strengths of association and the calculated strengths for these complexes to be 0.11, this may be the factor to reduce the calculated macrobond strengths (Table 4) to the real value for crystals in solution. This is consistent with the discussion in §4.2, where the hydration effect reduces the apparent magnitude of strength by a factor of 0.1. This factor also reduces the magnitude of $\gamma_{\rm vac}$ in Table 6 to several mJ m^{-2}, which is closer to the experimental value. By taking, for example, the average calculated macrobond strength of 200 kJ mol^{-1} for crystals in Table 4 and 800 kJ mol^{-1} for the enzyme–inhibitor in Table 7, both being the calculated values in vacuum, and using the relation $\Delta E = -RT\ln K_d$, the dissociation constant of the macrobond is calculated to be 2.6×10^{-4}. This value of the dissociation constant is about the same order as that for enzymes with weak substrates (Hiromi, 1988) or a weak antibody–antigen interaction (Eisen, 1980), which could be easily dissociated, for example upon dialysis. These results suggest that the strength of macrobonds in protein crystals is one of the weakest of the protein-interaction systems.

YM thanks Dr H. Hondoh for helpful discussions.

References

Antosiewicz, J., McCammon, J. A. & Gilson, M. K. (1994). *J. Mol. Biol.* **238**, 415–436.

Ataka, M. & Asai, M. (1988). *J. Cryst. Growth*, **90**, 86–93.

Berman, H. M., Westbrook, J., Feng, Z., Gilliland, G., Bhat, T. N., Weissig, H., Shindyalov, I. N. & Bourne, P. E. (2000). *Nucleic Acids Res.* **28**, 235–242.

Berthou, J., Lifchitz, A., Artymiuk, P. & Jolles, P. (1983). *Proc. R. Soc. London Ser. B*, **217**, 471–489.

Buckle, A. M., Schreiber, G. & Fersht, A. R. (1994). *Biochemistry*, **33**, 8878–8889.

Chernov, A. A. (1997). *Phys. Rep.* **288**, 61–75.

Cornell, W. D., Cieplak, P., Bayly, C. I., Gould, I. R., Merz, K. M., Ferguson, D. M., Spellmeyer, D. C., Fox, T., Caldwell, J. W. & Kollman, P. A. (1995). *J. Am. Chem. Soc.* **117**, 5179–5197.

Durbin, S. D. & Feher, G. (1991). *J. Cryst. Growth*, **110**, 41–51.

Eisen, H. N. (1980). *Immunology*, 2nd ed., ch. 16. Hagerstown: Harper & Rows.

Gilson, M. K. & Honig, B. (1988). *Proteins*, **4**, 7–18.

Hartman, P. (1973). *Crystal Growth: An Introduction*, edited by P. Hartman, ch. 14. Amsterdam: North-Holland.

Hiromi, K. (1988). In *Handbook of Amylases and Related Enzymes*, edited by the Amylase Research Society of Japan. Oxford: Pergamon Press.

Hodsdon, J. H., Brown, G. M., Sieker, L. C. & Jensen, L. H. (1990). *Acta Cryst.* B**46**, 54–62.

Hondoh, H., Sazaki, G., Miyashita, S., Durbin, S. D., Nakajima, K. & Matsuura, Y. (2001). *Cryst. Growth Des.* **1**, 327–332.

Huber, R., Kukla, D., Steigemann, W., Deisenhofer, J. & Jones, A. (1974). *Bayer-Symposium V 'Proteinase Inhibitors'*, edited by H. Fritz, H. Tschesche, L. J. Greene & E. Truscheit, pp. 497–512. Berlin: Springer–Verlag.

Ippolito, J. A., Alexander, R. S. & Christianson, D. W. (1990). *J. Mol. Biol.* **215**, 457–491.

Israelashvili, J. N. (1992). *Intermolecular and Surface Forces*, 2nd ed., p. 204. London: Academic Press.

Jeffrey, G. A. & Saenger, W. (1991). *Hydrogen Bonding in Biological Structures*, ch. 2. Berlin: Springer–Verlag.

Ko, T.-P., Day, J., Greenwood, A. & McPherson, A. (1994). *Acta Cryst.* D**50**, 813–825.

Kyte, J. (1995). *Structure in Protein Chemistry.* New York: Garland.

Lee, L.-P. & Tidor, B. (2001). *Nature Struct. Biol.* **8**, 73–76.

Madhusudan, Kodandapani, R. & Vijayan, M. (1993). *Acta Cryst.* D**49**, 234–245.

Malkin, A. J. & McPherson, A. (1994). *Acta Cryst.* D**50**, 385–395.

Monaco, L. A. & Rosenberger, F. (1993). *J. Cryst. Growth*, **129**, 465–484.

Nadarajah, A. & Pusey, M. L. (1996). *Acta Cryst.* D**52**, 983–996.

Oki, H., Matsuura, Y., Komatsu, H. & Chernov, A. A. (1999). *Acta Cryst.* D**55**, 114–121.

Rao, S. T. & Sundaralingam, M. (1996). *Acta Cryst.* D**52**, 170–175.

Reid, R. C., Prausnitz, J. M. & Sherwood, T. K. (1977). *The Properties of Gases and Liquids.* New York: McGraw–Hill.

Richards, F. M. (1977). *Annu. Rev. Biophys. Bioeng.* **6**, 151–176.

Rosenberger, F., Howard, S. B., Sowers, J. W. & Nice, T. A. (1993). *J. Cryst. Growth*, **129**, 1–12.

Sazaki, G., Nagatoshi, Y., Suzuki, Y. Durbin, S. D., Miyashita, S., Nakada, T. & Komatsu, H. (1999). *J. Cryst. Growth*, **196**, 204–209.

Strom, C. S. & Bennema, P. (1997*a*). *J. Cryst. Growth*, **173**, 150–158.

Strom, C. S. & Bennema, P. (1997*b*). *J. Cryst. Growth*, **173**, 159–166.

Vaney, M. C., Maignan, S., Riès-Kautt, M. & Ducruix, A. (1996). *Acta Cryst.* D**52**, 505–517.

Vekilov, P. G. & Chernov, A. A. (2002). *Solid State Phys.* **57**, 1–147.

Vincent, J.-P. & Lazdunski, M. (1972). *Biochemistry*, **11**, 2967–2977.

Wolfenden, R., Andersson, L., Cullis, P. M. & Southgate, C. C. B. (1981). *Biochemistry*, **20**, 849–855.